Volume 1 | Number 1 | Jan 2013 | Pages 1–100

Journal of
Materials Chemistry A

Materials for energy and sustainability
www.rsc.org/materialsA

Li⁺
e⁻
e⁻
Li⁺
Li⁺
Li⁺

ROYAL SOCIETY
OF CHEMISTRY

ROYAL SOCIETY
OF **CHEMISTRY**

www.rsc.org/materialsA

Mesoporous graphenes were synthesized via a template-assisted pyrolysis approach

and used as a material of porous diffusion layer for direct methanol fuel cell.

Journal of Materials Chemisty A
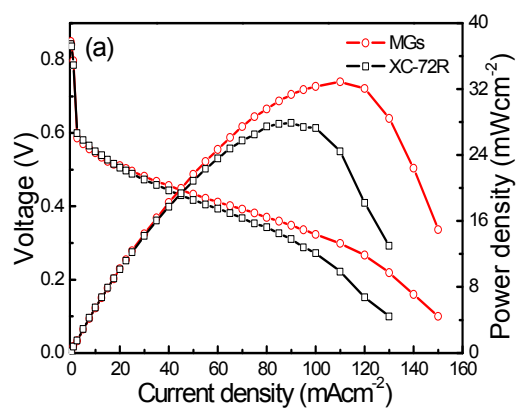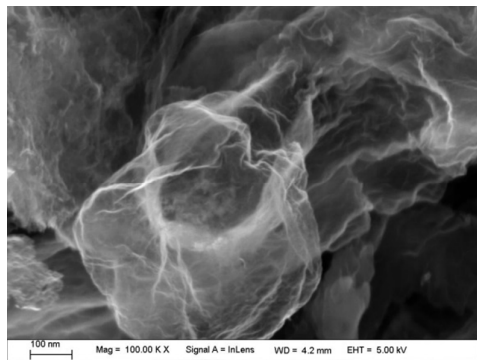
Full Papers

Facile preparation of mesoporous graphenes by sacrificial template approach for direct methanol fuel cell application

Jianyu Cao,[a,b] Hui Zhuang,[a] Mengwei Guo,[a] Hongning Wang,[a] Juan Xu,*[a] and Zhidong Chen*[b]

Mesoporous graphenes (MGs) were synthesized via a template-assisted pyrolysis approach and employed to fabricate the cathodic diffusion layer for direct methanol fuel cell (DMFC) application. Phenolic polymer-ammonium oleate supramolecular aggregates formed by weak acid-base interaction induced self-assembly and layered graphic carbon nitrides (g-C_3N_4) created under high temperature and a nitrogen 10 gas environment provide the solid carbon source and sacrificial template, respectively. The MGs are shown to have a specific mesopore surface area of 265.9 m^2 g^{-1} with large bimodal mesopore diameters of around 4 and 10 nm. Mesopores are generated by the in-situ formation and decomposition of g-C_3N_4 template. The passive DMFC fabricated by the use of MGs in the cathodic diffusion layer demonstrates a peak power density of 32.9 mW cm^{-2}, which is about 1.2 times higher than that with Vulcan XC-72R 15 carbons. The outstanding characteristics of MGs as a material of porous diffusion layer for DMFCs verify the great potential for use in energy-related fields.

Keywords: Mesoporous graphene; sacrificial template; diffusion layer; DMFC

Introduction

Direct methanol fuel cells (DMFCs) have attracted enormous 20 attention due to their impressive energy-conversion efficiency and high energy density, easy refuelling, long life, and low pollution along with increased concern over the depletion of fossil fuel resources.[1-3] Recently, extensive studies have shown that porous carbon materials such as activated carbons,[4] carbon 25 fibers,[5] carbon nanotubes,[6] and mesoporous carbons,[7] play an important role in determining the performance of a DMFC due to their unique nanoscale pore network and high electrical conductivity. In particular, effective surface area and appropriate pore size in the carbon nanostructure can effectively facilitate 30 transport of reactants[7] and access of the electrolyte[8] for better performance of the DMFC.

As a single layer of graphite, graphene recently has attracted a great deal of research interest in the field of energy conversion and storage. For examples, graphene has been widely recognized 35 as the promising support of fuel cell catalysts,[9, 10] and active materials of supercapacitors[11] and Li-ion batteries[12] due to its unique structure and superior physicochemical properties, such as excellent electrical conductivity, high theoretical specific surface area, good mechanical strength, and extraordinary chemical 40 stability. Unfortunately, during the preparation and drying process, graphene was usually suffering from restacking between individual graphene sheets due to the strong interlayer van der Waals forces, resulting in a dramatic decrease in the surface area

and pore volume. In addition, many graphene nanostructures 45 obtained from wet-chemical reduction[13-15] and chemical vapour deposition (CVD) growth approach[16, 17] often lack mesopores and macropores, despite having large surface area and great electrical conductivity. However, for electrocatalytic and/or electroactive materials, unique mesopore/macropore 50 characteristics can accelerate diffusion of reactive species, ions, and electrolytes to the electrode surface,[8, 18, 19] leading to improved performance. From this point of view, among the various methods available for the preparation of graphene materials, the template approach is highly recommended because 55 various mesopores/macropores can be effectively introduced and the pore structure can be tuned by simply adjusting the ratio of precursor/templating agent.

Herein, we report an effective route to obtain mesoporous graphenes (MGs) with large mesopore surface area and great 60 conductivity via a template-assisted pyrolysis approach. Phenolic polymer-ammonium oleate supramolecular aggregates formed by weak acid-base interaction induced self-assembly and layered graphic carbon nitrides (g-C_3N_4) created by the polycondensation of dicyandiamide under high temperature and a nitrogen gas 65 environment provide the solid carbon source and sacrificial template, respectively. The produced MGs present a high mesopore surface area (265.9 m^2 g^{-1}) and large bimodal mesopores (4 and 10 nm). The conductivity of MGs was measured to be 171.7 S cm^{-1}. The passive DMFC utilizing MGs 70 within the cathodic diffusion layer demonstrates an improved

performance and discharge stability. The excellent performance of MGs as the material of diffusion layer for DMFCs highlights its potential for use in energy-related fields.

Experimental methods

Materials

Dicyandiamide, 2,4-dihydroxybenzoic acid, and oleic acid were purchased from Sigma-Aldrich. Methanol, formaldehyde (37 wt.%), and ammonium hydroxide (28 wt.% NH_3) were obtained from Sinopharm Chemical Reagent Co. Ltd. Vulcan XC-72R carbons were purchased from Cabot. All chemicals were used as received without further purification.

Preparation of mesoporous graphenes

MGs were synthesized based on a weak acid-base interaction induced self-assembly [20] and subsequent sacrificial-template-assisted pyrolysis approach. [21] Typically, 2.5 mmol of 2,4-dihydroxybenzoic acid and 7.5 mmol of formaldehyde were firstly dissolved in 95 mL of ultrapure water. Then, a aqueous solution (5 mL) containing 56 μL of oleic acid and 160 μL of ammonium hydroxide solution (28 wt.%) was added to the above solution under slow stirring at 30 °C. The mixture solution was stirred for 30 min to yield a stable phenolic polymer emulsion. After 5.3 g of dicyandiamide being added and stirring for 3 h, the solvent was removed by rotary evaporation at 60 °C. The yellow powders were obtained after drying in an oven at 70 °C for 24 h and acted as the precursor for MGs. Finally, MGs were obtained by heating the precursor to 1000 °C and holding it at that temperature for 1 h under a nitrogen atmosphere. In this procedure, the heating rate before and after 600 °C is 2 and 3.3 °Cmin^{-1}, respectively.
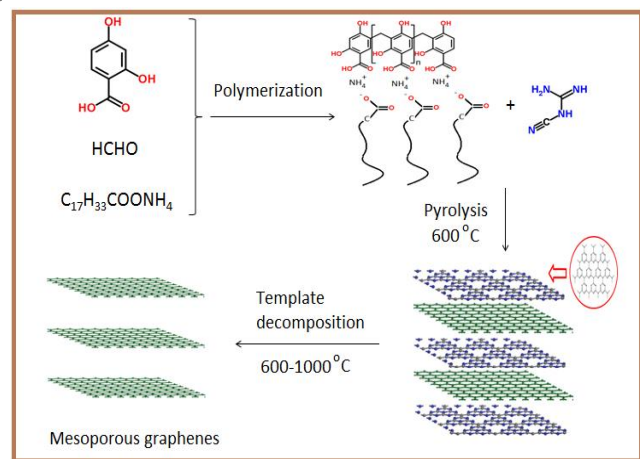

Fig. 1 Schematic illustration for the synthesis of MGs.

Preparation of MEAs

Nafion115 membrane was used as the electrolyte and its pre-treatment procedures were described in our previous work. [22] The pre-treated membranes were kept in ultrapure water prior to the fabrication of membrane electrode assemblies (MEAs). Toray carbon paper (TGPH060, 20 wt.% wet-proofed) was used as the anodic backing layer. A slurry of Vulcan XC-72R carbons and polytetrafluoroethene (PTFE), consisted of 20 wt.% PTFE with a 1.0 ± 0.1 mg cm^{-2} carbon loading, was coated onto the

carbon paper to form the anodic diffusion layer (ADL). For the cathode side, the carbon cloth (Type A, 10 wt.% wet-proofed) was used as the cathodic backing layer. A slurry of MGs and PTFE, consisted of 20 wt.% of PTFE with a 2.0 ± 0.2 mg cm^{-2} carbon loading, was coated onto the carbon cloth to form the cathodic diffusion layer (CDL), herein labelled as MG-CDL. For the comparison, a conventional CDL with Vulcan XC-72R carbon was obtained using a same procedure, which was labelled as XC-CDL. The catalyst ink was prepared by mixing a given amount of catalyst with 5 wt.% Nafion solution (DuPont), isopropyl alcohol and water. After ultrasonically dispersed for at least 3 h at room temperature, the above catalyst ink was sprayed onto the surface of the diffusion layer to form the gas diffusion electrode. Here, a mixture of Pt-Ru (1:1) black (HiSPEC™ 6000, Johnson Matthey) and Pt-Ru (1:1)/C (HiSPEC™ 10000) with a mass ratio of 3:5 was used as the anode catalyst, while Pt/C (HiSPEC™ 9100) was used as the cathode catalyst. The metal loadings are 4.0 ± 0.2 mg cm^{-2} and the Nafion content is 20 wt. % for both the anode and cathode. Finally, an MEA with 4 cm^2 active surface area was obtained by hot-pressing the anode and cathode onto a pre-treated Nafion 115 membrane at 6 MPa and 130 °C for 3 min.

Characterization

The morphology of MGs was observed by the field emission scanning electron microscope (FESEM, Supra 55, Carl Zeiss), transmission electron microscope (TEM, JEM-2100, JEOL), and atomic force microscope (AFM, Multimode V, Veeco) respectively. For TEM characterization, the samples were ultrasonically dispersed in ethanol to obtain uniform ink. Then, a drop of ink was mounted onto copper grids covered with holey carbon film and dried in the air. The AFM was operated in the tapping mode using silicon cantilevers with a force constant of 40 N m^{-1}. X-ray diffraction (XRD) measurements were carried out with a Rigaku D/max-2500 diffractometer with a Cu Kα radiation ($\lambda = 0.15418$ nm). Diffraction patterns were collected at a scanning rate of 2° min^{-1} and with a step of 0.02 °. Nitrogen adsorption-desorption isotherms of MGs were measured at 77 K using a surface area analyzer (ASAP 2010 Micromeritics). Before measurements, the sample was degassed in a vacuum at 200 °C for at least 6 h. The specific surface area and pore volume were determined using the Brunauer-Emmett-Teller (BET) method and the single point method, respectively. Pore size distribution curves were obtained by Barrett-Joyner-Halenda (BJH) method. The electrical conductivity of MGs was measured with a powder resistivity meter (FZ-9601, Shanghai Xiyu Co. Ltd.) by confining the pressed MG powders between two metal discs. During the conductivity measurement, a pressure of 2 MPa is applied to ensure good electrical contacts between carbon grains. Evaluation of the electronic structure and surface composition for MGs was conducted with an X-ray photoelectron spectroscopy (Escalab 250, Thermo Scientific) using Al Kα radiation. The binding energy was referenced to the C1s spectrum at 284.5 eV. The Raman spectrum was collected by using Raman microscope (DXR, Thermo Scientific) under the 514 nm excitation. The FTIR spectrum was recorded in the range from 4000 to 400 cm^{-1} with a spectral resolution of 0.1 cm^{-1} using a Nexus 670 FTIR spectrometer (Thermo Nicolet).

Single cell testing

For DMFC test, the MEA was sandwiched between two gold-plated current collectors. The polarization curves were obtained on a fuel cell testing system (Arbin) under a passive operation using 3 M methanol solution. For each discharging current point along a polarization curve, a wait of 2 minutes is selected to obtain the stable voltage reading. The discharging tests of passive DMFCs were operated at a constant current density of 40 mA cm^{-2}.

Electrochemical measurements

Electrochemical impedance spectra (EIS) were measured on a Solartron Impedance/Gain-phase analyzer (Model 1260A) controlled by a personal computer with Corrware software (Scribner Associates, Inc.). The impedance spectra were acquired at a given direct-current (DC) potential of 0.5 V in the frequency range from 10 kHz to 10 mHz, with the amplitude of the sinusoidal voltage signal less than 10 mV. The obtained impedance spectra were analysed on the basis of an electrical circuit element model. The fitting errors were kept within 10%.

Results and discussion

The synthesis procedure is illustrated in Fig. 1. An emulsion was formed by mixing ammonium oleate, 2,4-dihydroxybenzoic acid, and formaldehyde solution. Ammonium ions may bridge oleic acid and 2,4-dihydroxybenzoic acid by weak acid-base interactions and lead to the formation of phenolic polymer-ammonium oleate supramoleculars in the polymerization process.[20] In the following pyrolysis, as the temperature rises from room temperature to ~600 °C, the polymerization of dicyandiamide undergoes a series of nitrogen-containing polymer (eg. melamine, melem, melon and so on [23]) and finally leads to g-C$_3$N$_4$ polymers, accompanying with pyrolysis of phenolic polymer to form layered graphene sheets. When the temperature is further increased from 600 to 1000 °C, abundant mesopores can be created due to rapid decomposition of g-C$_3$N$_4$ template between graphene sheets.

Fig. 2 presents the morphological observation of MGs created by sacrificial template method. The FESEM images in Fig. 2a and 2b reveal that MGs have a highly porous morphology and entangled, transparent, three-dimensional nanosheets with macroporous networks and mesoporous channels are observed clearly. The diameter of these open pores ranges from 10 nm up to several hundred nanometers. Unlike chemically reduced graphenes obtained from graphene oxides, which usually suffer extended aggregation into thick sheets, [24] the primary nanosheets in MGs are thin and very flexible, the wall thickness of which is within a few nanometers. TEM characterization (shown in Fig. 2c and 2d) indicates the typical wrinkles of oligolayered graphenes. A detailed inspection for MGs in Figure 2c reveals that the width of the nanosheets ranges 500-600 nm and the thickness does not exceed 5 nm. The high resolution TEM image of MGs presented in Fig. S1 further confirms the formation of multilayer graphene with the layer thickness of 2-4 nm. The representative AFM image of MGs was shown in Fig. 3, which gives a single graphene nanosheet deposited on the silicon wafer. The height profile in the right of Fig. 3 shows that the thickness of the nanosheet is ~4 nm, indicating that the as-obtained graphene nanosheet is few-layered, which is in good agreement with the results of the TEM observation.
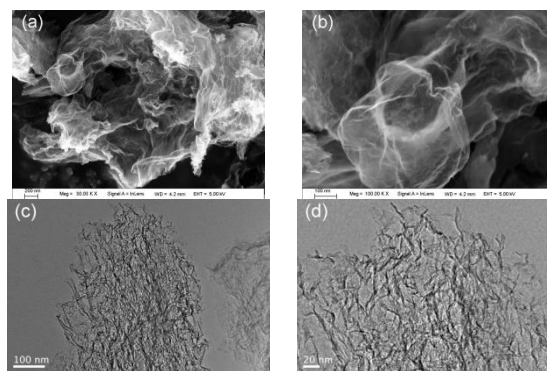

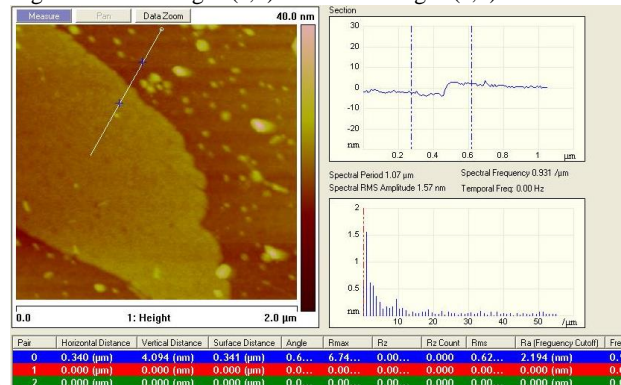Fig. 2 FESEM images (a,b) and TEM images (c,d) of MGs.

Fig. 3 Typical AFM image of MGs. The curve in the upper right panel show the height and width information of graphene nanosheets from the AFM image.

The XRD was used to determine the crystalline structure of MGs. Fig. 4 displays XRD patterns of MGs and graphite. A broad diffraction peak at $2\theta = 26°$ corresponding to the (002) plane of graphitic carbon appears at the XRD pattern of MGs, indicating the successful formation of graphitic aromatic structure in MGs owing to the high-temperature pyrolysis of phenolic polymer. As compared to the sharp (002) peak of graphite, the (002) peak of MGs is quite weaker and broader, demonstrating that graphene sheets in MGs are loosely stacked, which is derived from g-C$_3$N$_4$ template that is formed during the high-temperature calcination is then decomposed at a higher temperature, in good accordance with SEM and TEM images. According to Bragg's law, the interlayer spacing (d_{002}) is calculated to be about 0.342 nm for MGs, slightly broader than those of well-ordered bulk graphite (0.335 nm). In addition, as for MGs, a small (100) peak (the inset of Fig. 4) can be observed, indicating fairly high graphitization agree.[25]
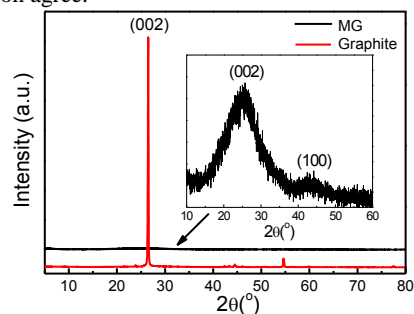

Fig. 4 XRD patterns of MGs and graphite.

N$_2$ adsorption-desorption isotherms of MGs in Fig. 5a show a typical type IV curve with a large H2 hysteresis loop, indicating

the existence of mesopores. These mesopores are generated by the in-situ formation and decomposition of g-C_3N_4 template. [21] However, the isotherms for graphenes (Grs) that were synthesized without using dicyandiamide exhibits a typical type I isotherm, where the main adsorption occurs at low relative P/P_0 pressures, which is a characteristic of microporous materials. [26] The textural properties of two samples are summarized in Table 1. The specific surface area of MGs is calculated to be 283.4 m^2 g^{-1}, slightly higher than that of the 2D mesoporous graphene nanosheets reported previously [27] while this data is significantly lower than that of the graphenes obtained without using dicyandiamide. Mesopore surface area for MGs reaches to 265.9 m^2 g^{-1} and the mesopore content (the ratio of mesopore volume to total pore volume) is ca. 98.6%, indicating that MGs consist mainly of mesopores. The total pore volume for MGs is estimated to be ca. 0.70 cm^3 g^{-1}, much larger than that of Grs, which is attributed to the existence of abundant mesopores in MGs. The mesopore volume for MGs is ca. 0.69 cm^3 g^{-1}, much larger than that of Grs (0.17 cm^3 g^{-1}), indicating that dicyandiamide plays an important role in forming mesoporous structure, since those graphenes obtained without using dicyandiamide exhibit much less mesopore volume than that of MGs. The BJH pore size distribution (Fig. 5b) indicates that MGs possess a relatively narrow pore size distribution with a sharp peak at 4 nm and a flat peak at 10 nm, respectively. In contrast, no peak of pore size distribution is observed in the curve of Grs. These results demonstrate again the important role of g-C_3N_4 sacrificial template in the formation of the mesoporous graphene structure. Table 1 reveals an average pore diameter of 9.3 nm for MGs, calculated through the desorption isotherm, which is much larger than that of Grs (3.1 nm). Such large average pore size is uncommon for graphene materials (the average pore size of chemically reduced graphene oxides is 2~6 nm with a wide pore size distribution [25, 28]) and can be ascribed to the use of g-C_3N_4 sacrificial template in the pyrolysis synthesis. It is noted that the graphenes reported by Li et al. [21], which were synthesized using glucose as the carbon source and dicyandiamide as the precursor of template, do not exhibit distinctive characteristics of mesoporous materials. However, in our work, phenolic polymer-ammonium oleate supramolecular as a carbon source which is much larger than glucose, can more effectively wrap dicyandiamide and form strong intermolecular interactions, thus facilitating the formation of mesoporous structure in high-temperature pyrolysis. The bulk electrical conductivity of MGs was determined to be ca. 171.7 S cm^{-1}, which is much higher than that reported for mesoporous graphene nanoballs prepared by chemical vapour deposition. [11]

Table 1 Textural properties of MGs and Grs.

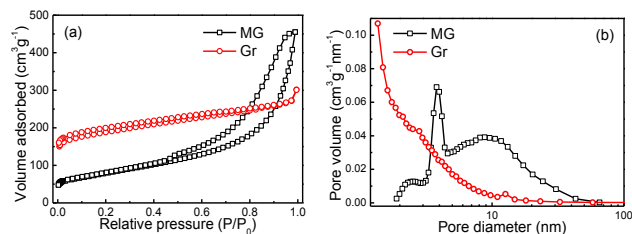| Sample	S_{BET} (m^{2}g^{-1})	S_{meso} (m^{2}g^{-1})	V_{meso} (cm^{3}g^{-1})	V_{pore} (cm^{3}g^{-1})	d_{BJH} (nm)
MG	283.4	265.9	0.69	0.70	9.3
Gr	701.2	227.3	0.17	0.47	3.1

Fig. 5 N$_2$ adsorption-desorption isotherms (a) and BJH pore size distribution curves (b) for MGs and graphenes obtained without using dicyandiamide in the synthesis process.

The wide survey XPS spectrum (Fig. 6a) of MGs reveals the presence of C, N, and O elements. The total nitrogen and oxygen contents of MGs were calculated from XPS to be 2.04% and 19.57%, respectively. The high content of foreign atoms (including N and O) may in part be due to the presence of surface-absorbed water and other small molecules since such high-surface-area carbons are superadsorbing materials. [21] The high-resolution C 1s spectrum (Fig. 6b) displays three different peaks at 284.5, 286.1, and 288.6 eV, corresponding to C=C-C (sp2 C), C-O/C-N, and C=O groups, respectively. The high-resolution N 1s scan (Fig. 6c) indicates the presence of three forms of nitrogen, namely, pyridinic N (397.5 ± 0.2 eV), pyrrolic N (400.3 ± 0.2 eV), and graphitic N (401.5 ± 0.2 eV). [29] The nitrogen content of MGs can be controlled and adjusted by the amount of dicyandiamide and heating temperature. Raman spectroscopy is an effective technique to investigate the structural changes of graphene layers. The Raman spectrum of MGs is shown in the Fig. S2. The peak located at ca. 1370 cm^{-1} is the D band related to the edges, defects and structural disorders in MGs. The G band around 1570 cm^{-1} arises from the first-order scattering of E_{2g} mode of sp^2 carbon. The intensity ratio of two bands (I_D/I_G) is used widely to prove the graphitization degree of carbon materials. A lower value represents a higher degree of graphitization. [30] The MGs show an I_D/I_G value of ~0.97, much lower than those of the graphene materials obtained from chemical reduction of graphene oxide (I_D/I_G = ~2.4) [31], indicating that MGs synthesized from sacrificial template approach possess a higher graphitization degree and relatively fewer defects. In addition, the sharp peak at 2330 cm^{-1} can be assigned to the fundamental vibration of surface-attached N$_2$ molecules. [32] The FTIR spectrum of MGs is shown in Fig. S3. The sharp peaks of moderate intensity at 2362 and 2332 cm^{-1} can correspond to the presence of residual nitrile group (C≡N) on the surface of sample. [33] The absorption band near 1688 cm^{-1} confirms the presence of C=O groups. [34] The absorption band at ca. 1637 cm^{-1} can be assigned to skeletal vibrations of C=C and/or C=N of graphitic domains. [34, 35] The band at 1400 cm^{-1} might be from the deformation vibrations of the OH groups on the surface of MGs [36] and the band at ca. 738 cm^{-1} associates with C-H out of plane deformation. [37]
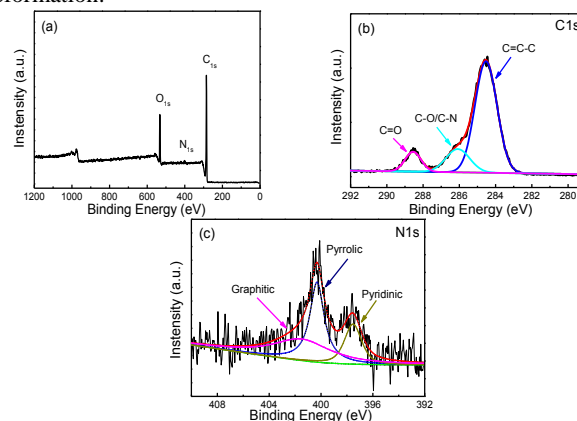

Fig. 6 XPS survey spectrum of MGs, with the C 1s and N 1s spectra.

Taking into account MGs synthesized from sacrificial template approach not only have a high electrical conductivity but also

possess abundant mesoporous structures that are beneficial to promote mass transfer in the electrode/electrolyte interface, we have employed MGs to fabricate the cathodic diffusion layer for passive DMFCs. For a fair comparison, the same amount of MGs and XC-72R carbons were coated onto the backing layer (porous substrate), respectively, to form the cathodic diffusion layer. Fig. 7a compares the polarization curves of two passive DMFCs utilizing MGs and XC-72R carbons within the CDL, respectively. It can be observed that, in low current density region, two passive DMFCs exhibit similar kinetic and ohmic polarization due to similar catalyst layers were used. However, in high current density, the polarization curve of the passive DMFC with MGs shows a smaller voltage drop compared with that with XC-72R carbons. The maximum power density for the passive DMFC with MGs is ca. 32.9 mW cm^{-2}, which is about 1.2 times higher than that with XC-72R (27.9 mW cm^{-2}). The discharge curves (Fig. 7b) for passive DMFCs utilizing MGs and XC-72R within the CDL, respectively, are compared under a constant current density of 40 mA cm^{-2}. It can be seen that the passive DMFC with MGs shows a higher and more stable cell-voltage than that with XC-72R. The Faraday efficiency and energy efficiency for the passive DMFC with MGs are calculated to 42.0% and 13.8%, respectively, which is much higher than those of the passive DMFC with XC-72R (33.8% and 10.7%). To clarify the effect of MGs within the cathodic diffusion layer on cell performance, EIS for two MEAs was analysed. Fig. S4 shows the experimental impedance spectra and the simulation data based on an equivalent circuit presented in Fig. S4b for the passive DMFCs employing MGs and XC-72R in the CDL, respectively. The fitting results are in good agreement with the experimental data essentially over the full range of frequencies and fitting parameters are listed in Table S1. The passive DMFC with MGs possesses a much lower charge-transfer resistance (R_{ct-c}, 0.405 Ω) than that with XC-72R (0.825 Ω) for cathodic oxygen reduction, indicating that the adoption of MGs in the cathodic diffusion layer results in a significant decrease of charge-transfer resistance. It is well known that for electrochemical reactions involving gases or liquids, increasing the concentration of electroactive reactant increases the charge-transfer rate, which would result in the acceleration of the electrochemical reaction and the improvement of cell performance. Therefore, the probable reason for the decreased charge-transfer resistance is that MGs within the CDL facilitates oxygen diffusion, leading to an increased oxygen concentration, which might explain the improved performance of the passive DMFC with MGs, as shown in Fig. 7.
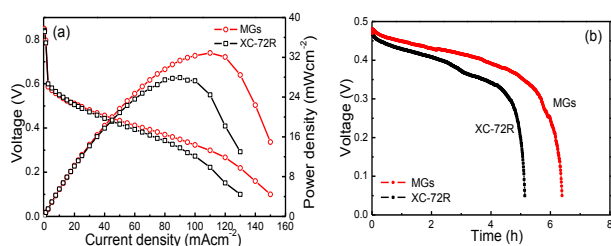

Fig. 7 Polarization curves (a) and discharge curves under a current density of 40 mA cm^{-2} (b) for the passive DMFCs utilizing MGs and Vulcan XC-72R carbons within the CDL, respectively, fed with a 3 M methanol solution at 25 °C.

Conclusions

We have developed an effective method for fabrication of mesoporous graphenes from a phenolic polymer precursor via a template-assisted pyrolysis process. Mesopores are generated by the in-situ formation and decomposition of g-C$_3$N$_4$. The mesoporous graphenes exhibit large specific mesopore surface area and high bulk conductivity. The passive DMFC utilizing MGs within the cathodic diffusion layer shows good performance and discharge stability. The outstanding performance of MGs as a material of porous diffusion layer for DMFCs highlights its potential in energy-related applications.

Acknowledgments

Notes and references

a Jiangsu Key Laboratory of Advanced Catalytic Materials and Technology, Changzhou University, 1 Gehu Road, Changzhou 213164, PR China. Fax: 86 0519 86330239; Tel: 86 0519 86330239; E-mail: cjytion@163.com (J.Xu)

b Key Laboratory for Solar Cell Materials and Technology of Jiangsu Province, Changzhou University, 1 Gehu Road, Changzhou 213164, PR China. Fax: 86 0519 86450008; Tel: 86 0519 86450008; E-mail: jyucao@gmail.com (Z. Chen)

† Electronic Supplementary Information (ESI) available: [details of any supplementary information available should be included here]. See DOI: 10.1039/b000000x/

‡ Footnotes should appear here. These might include comments relevant to but not central to the matter under discussion, limited experimental and spectral data, and crystallographic data.

1   X. Ren, T.E. Springer, and S. Gottesfeld, J. Electrochem. Soc., 2000, **147**, 92.

2   Y.-H. Cho, N. Jung, Y.S. Kang, D.Y. Chung, J.W. Lim, H. Choe, Y.-H. Cho, and Y.-E. Sung, Int. J. Hydrogen Energy, 2012, **37**, 11969.

3   M. Chen, J. Chen, Y. Li, Q. Huang, H. Zhang, X. Xue, Z. Zou, and H. Yang, Energy Fuels, 2012, **26**, 1178.

4   G. Wang, G. Sun, Q. Wang, S. Wang, J. Guo, Y. Gao, and Q. Xin, J. Power Sources, 2008, **180**, 176.

5   S.-M. Park, D.-H. Jung, S.-K. Kim, S. Lim, D. Peck, and W.H. Hong, Electrochim. Acta 2009, **54**, 3066.

6   T. Yuan, Z. Zou, M. Chen, Z. Li, B. Xia, and H. Yang, J. Power Sources, 2009, **192**, 423.

7   J. Cao, L. Wang, L. Song, J. Xu, H. Wang, Z. Chen, Q. Huang, and H. Yang, Electrochim. Acta, 2014, **118**, 163.

8   B. Xu, L. Shi, X. Guo, L. Peng, Z. Wang, S. Chen, G. Cao, F. Wu, and Y. Yang, Electrochim. Acta 2011, **56**, 6464.

9   S.-S. Li, J.-J. Lv, Y.-Y. Hu, J.-N. Zheng, J.-R. Chen, A.-J. Wang, and J.-J. Feng, J. Power Sources, 2014, **247**, 213.

10   Z.-S. Wu, S. Yang, Y. Sun, K. Parvez, X. Feng, and K. Müllen, J. Am. Chem. Soc., 2012, **134**, 9082.

11   J.-S. Lee, S.-I Kim, J.-C. Yoon, and J.-H. Jang, ACS Nano, 2013, **7**, 6047.

12   E.J. Yoo, J. Kim, E. Hosono, H.-S. Zhou, T. Kudo, and I. Honma, Nano Lett., 2008, **8**, 2277.

13   Z. Lei, L. Lu, and X.S. Zhao, Energ. Environ. Sci., 2012, **5**, 6391.

14   L.L. Zhang, X. Zhao, M.D. Stoller, Y. Zhu, H. Ji, S. Murali, Y. Wu, S. Perales, B. Clevenger, and R.S. Ruoff, Nano Lett., 2012, **12**, 1806.

15 K.C. Kemp, V. Chandra, M. Saleh, and K.S Kim, Nanotechnology, 2013, **24**, 2357031.

16 V. Presser, M. Heon, and Y. Gogotsi, Adv. Funct. Mater., 2011, **21**, 810.

5 17 Z. Chen, W. Ren, L. Gao, B. Liu, S. Pei, and H.-M. Cheng, Nat. Mater., 2011, **10**, 424.

18 L. Gueudré, M. Milina, S. Mitchell, and J. Pérez-Ramírez, Adv. Funct. Mater., 2014, **24**, 209.

19 Z. Yan, M. Zhang, J. Xie, H. Wang, and W. Wei, J. Power Sources, 10 2013, **243**, 48.

20 G.-H. Wang, Q. Sun, R. Zhang, W.-C. Li, X.-Q. Zhang, and A.-H. Lu, Chem. Mater. 2011, **23**, 4537.

21 X.-H. Li, S. Kurasch, U. Kaiser, and M. Antonietti, Angew. Chem. Int. Ed., 2012, **51**, 9689.

15 22 J. Cao, M. Chen, J. Chen, S. Wang, Z. Zou, Z. Li, D.L. Akins, and H. Yang, Int. J. Hydrogen Energy, 2010, **35**, 4622.

23 K.K. Han, C.C. Wang, Y.Y. Li, M.M. Wan, Y. Wang, J.H. Zhu, RSC Adv., 2013, **3**, 9465.

24 Z.H. Sheng, L. Shao, J.-J. Chen, W.-J. Bao, F.-B. Wang, and X.-H. 20 Xia, ACS Nano, 2011, **5**, 4350.

25 J. Yan, Y. Xiao, G. Ning, T. Wei, and Z. Fan, RSC Adv., 2013, **3**, 2566.

26 Z.-H. Huang, G. Liu, F. Kang, ACS Appl. Mater. Inter., 2012, **4**, 4912-4917.

25 27 Y. Fang, Y. Lv, R. Che, H. Wu, X. Zhang, D. Gu, G. Zheng, and D. Zhao, J. Am. Chem. Soc., 2013, **135**, 1524.

28 K.-S. Kim, S.-J. Park, Electrochim. Acta, 2011, **56**, 6547.

29 Y. Shao, S. Zhang, M.H. Engelhard, G. Li, G. Shao, Y. Wang, J. Liu, I.A. Aksay, and Y. Lin, J. Mater. Chem., 2010, **20**, 7491.

30 30 X. Wen, D. Zhang, T. Yan, J. Zhang, L. Shi, J. Mater. Chem. A, 2013, **1**, 12334.

31 G. Wang, J. Yang, J. Park, X. Gou, B. Wang, H. Liu, J. Yao, J. Phys. Chem. C, 2008, **112**, 8192.

32 M. Roskosz, B.O. Mysen, and G.D. Cody, Geochim. Cosmochim. 35 Acta, 2006, **70**, 2902.

33 S.C. Ray, A. Saha, N.R. Jana, and R. Sarkar, J. Phys. Chem. C, 2009, **113**, 18546.

34 P.D. Kale, J. Chem. Pharm. Res., 2013, **5**, 130.

35 N.G. Sahoo, H. Bao, Y. Pan, M. Pal, M. Kakran, H.K.F. Cheng, L. 40 Li, and L.P. Tan, Chem. Commun., 2011, **47**, 5235.

36 Y. Tang, D. Wu, S. Chen, F. Zhang, J. Jia, and X. Feng, Energ. Environ. Sci., 2013, **6**, 2447.

37 H. Shirakawa, S. Ikeda, Polym. J., 1971, **2**, 231.